Theoretical Response of a Simply Supported Beam with a Strain Rate Dependant Modulus to a Moving Load

H. Aied[a] and A. Gonzalez[a,*]

[a]*School of Civil, Structural and Environmental Engineering, University College Dublin, Dublin, Ireland*

[*]corresponding author: arturo.gonzalez@ucd.ie

ABSTRACT

Moving load problems typically consider a structural material with properties that do not vary while the load traverses the structure. However, there is evidence that for some materials the structure will respond with a higher modulus of elasticity than that corresponding to a static test for sufficiently high strain rates. This paper investigates the variation in strain rate of a simply supported beam made of a viscoelastic material traversed by a moving load and its effect on the modulus of elasticity. The influence of speed and magnitude of the moving load on the displacement and strain responses of the beam is discussed.

Keywords: Moving load, strain rate, modulus of elasticity, viscoelasticity

1- Introduction

Large dynamic loads that are applied very rapidly, such as impact loading, have been shown to largely influence the way a structural material behaves [1-6]. Modulus of elasticity, and tensile and compressive strengths are some of the material properties affected by the dynamic nature of the applied load. This phenomena is commonly found in construction materials such as asphalt [7] or concrete [1, 5], which loaded at constant strain rate, exhibit significant increases in the modulus of elasticity as strain rate is raised. In the case of reinforced concrete tests, the increase in modulus of elasticity with strain rate strongly depends on the method of testing [3, 8]. No significant increase is identified for steel [8-10]. In addition to impact studies, differences between the 'static' modulus of elasticity, E_s, (i.e., derived from static loading tests) and the 'dynamic' modulus, E_d, are also noticeable when the latter is derived from measured frequencies of vibration [11]. Different analytical techniques (eigenvalue analysis, Rayleigh energy method) are employed to derive a relationship between frequency and E_d [12]. Finally, simple equations such as "$E_s = 0.83E_d$" and "$E_s = 1.25E_d$ -19 (both E_s and E_d in GPa)" are proposed for concrete by Lydon and Balendran [13] and BSI [14] respectively [15].

It is then acknowledged that high strains can lead to a 'dynamic' modulus significantly different from the 'static' modulus. Two questions arise here: (i) "what's the static strain rate threshold beyond which the material will start to develop viscoelastic properties?" and (ii) "how E_d relates to E_s at high strain rates?". In relation to the first question, Bischoff and Perry

[2] consider that strain rates can vary from 10^{-6} s^{-1}, for the case of a static load application, to 10^{3} s^{-1} for hard impact or an explosion. For loads moving across a structure, the strain rate will depend on the mechanical properties of the structure, the magnitude and speed of the load, but it can be assumed to be somewhere between the static ($>10^{-6}$ s^{-1}) and that associated to earthquake loading ($<10^{-2}$ s^{-1}). The response of a beam to a moving load has been investigated for numerous scenarios in the literature: uniform and tapered sections [16], straight and curved alignments [17], simple supported and continuous spans [18], un-cracked and cracked sections [19, 20], Euler-Bernoulli and Timoshenko type [21], etc. A thorough review can be found in [22-26] . However, these moving load investigations use material properties that do not vary during the load crossing; in particular, the influence of strain rate on the behaviour of the material is neglected. While the latter will hold true for some materials or applications of small loads at low speeds, recent research confirms the impact of high strain rate on the properties of concrete in bridges [1, 2, 27]. Further evidence can be found in the Bridge Weigh-In-Motion literature, where the static moment in a bridge is related to the measured strain (prior removal of dynamics and noise via a low-pass filter) by scaling the influence line using a calibration factor. The calibration factor is representative of the section modulus and modulus of elasticity at the measurement point and it is obtained by driving a vehicle(s) of known configuration with different speeds and loading conditions over the bridge. However, some Bridge Weigh-In-Motion sites have revealed a tendency of the factor to increase with higher loads and speeds [28]. These sites suggest that the mechanical properties of the bridge are affected by high strain rates and are one of the drivers for the theoretical investigations in this paper. By the first time in the literature, consideration is given to how the strain rate and modulus of elasticity of a beam made of a viscoelastic material change over time due to a moving load. Given that E_d is higher than E_s, as strain rate rises, the structure will behave in a stiffer way and react to the applied load with a smaller response than initially expected. Simulations are carried out for simply supported beams with different mechanical properties. Load speeds and load magnitudes are also varied in order to assess the impact of introducing a viscoelastic material in the moving load problem.

2- Model to Simulate the Response of a Beam to a Moving Load

The moving load is represented by a constant force and the underlying structure is modelled as a simply supported discretized finite element Euler-Bernoulli beam of constant rectangular cross-section as sketched in Fig. 1.

Although this simplistic model assumes that the mass of the moving load is much smaller than that of the bridge (i.e., the interaction between both is neglected), it is still widely used in research and in practice. For instance, it has resembled patterns of dynamic amplification versus speed measured in bridges [20]. Therefore, it is deemed to be sufficient for the aim of evaluating the strain rate that may develop in the beam and its potential effect on the overall response. Details on its implementation [29] are provided here.

Fig. 1. Simulation model

Two degrees of freedom per beam node are considered in this model (vertical displacement u_j and rotation θ_j for each elementary beam j as shown in Fig. 2). Therefore, the elementary stiffness matrix [K_j] relating forces and moments to these degrees of freedom at each individual discretized beam j is given by:

$$\left[K_j\right] = \begin{bmatrix} \frac{12E_jI_j}{L_j^3} & \frac{6E_jI_j}{L_j^2} & -\frac{12E_jI_j}{L_j^3} & \frac{6E_jI_j}{L_j^2} \\ \frac{6E_jI_j}{L_j^2} & \frac{4E_jI_j}{L_j} & \frac{6E_jI_j}{L_j^2} & \frac{2E_jI_j}{L_j} \\ -\frac{12E_jI_j}{L_j^3} & -\frac{6E_jI_j}{L_j^2} & \frac{12E_jI_j}{L_j^3} & -\frac{6E_jI_j}{L_j^2} \\ \frac{6E_jI_j}{L_j^2} & \frac{2E_jI_j}{L_j} & -\frac{6E_jI_j}{L_j^2} & \frac{4E_jI_j}{L_j} \end{bmatrix} \quad (1)$$

where E_j, L_j, and I_j are the modulus of elasticity, length, and second moment of area of each elementary beam. These elementary stiffness matrixes are assembled into the global stiffness matrix [K] (Fig. 1).

Initially, the modulus of elasticity E_j is adopted to be the 'static' modulus E_s. However, in the case of using a strain rate dependant material, the modulus of elasticity E_j (and hence, the stiffness E_jI_j) may adopt a value of 'dynamic' moduli E_d that can vary at each point in time. These changes in stiffness are updated using an equivalent moment of inertia as follows. The cross-section of each elementary beam is discretised into strips as in Fig. 2. In this figure, d is the depth of each strip, which has been adopted to be 0.003 m for the simulations in this paper (i.e., 200 strips for a total element depth of 0.60 m).

Fig. 2. Elementary beam element: a) Elevation, b) cross-section

The displacements of the beam at each node are calculated using the equation of motion in Fig. 1 and the strain $\varepsilon_{j,k}$ is estimated using Equation (2) for each k^{th} strip of beam element j at each time step:

$$\varepsilon_{j,k} = \frac{-y_k}{L_j^3}\left\{\left(6L_j - 12x_e\right)\ \left(4L_j^2 - 6L_j x_e\right)\ \left(-6L_j + 12x_e\right)\ \left(2L_j^2 - 6L_j x_e\right)\right\}\begin{Bmatrix} u_j \\ \theta_j \\ u_{j+1} \\ \theta_{j+1} \end{Bmatrix} \quad (2)$$

where y_k is the distance from the centre of the k^{th} strip to the neutral axis of the entire cross-section and x_e is the distance where strain is obtained at the beam element. The value $x_e = L_j / 2$, where L_j is the length of the beam element, is used in the simulations to calculate an average strain for each element. Strains from Equation (2) are then used to derive the strain rate $\dot{\varepsilon}_{j,k}$ for each element *j* and strip *k* (Equation (3)):

$$\dot{\varepsilon}_{j,k}(t) = \left(\frac{\varepsilon_{j,k}(t) - \varepsilon_{j,k}(t - \Delta t)}{\Delta t}\right) \quad (3)$$

where Δt is the time increment. This strain rate is used to calculate the 'dynamic' modulus E_d corresponding to each strip *k* using Equation (4) which relates E_d to E_s and $\dot{\varepsilon}$:

$$\begin{cases} E_d(t) = E_s\left(\dfrac{\dot{\varepsilon}_{j,k}(t)}{\dot{\varepsilon}_0}\right)^{\gamma} \text{ for } \dot{\varepsilon}_k > \dot{\varepsilon}_0 \\ E_d = E_s \text{ for } \dot{\varepsilon}_k \le \dot{\varepsilon}_0 \end{cases} \quad (4)$$

Here $\dot{\varepsilon}_0$ is 'static' strain rate threshold (or value in s^{-1} above which the modulus becomes strain rate dependant) and γ is an empirical constant. In Equation (4), E_s is the 'static' modulus of elasticity (N/m^2). This equation is a typical constitutive model for viscoelastic materials, which has been adopted by the Comité Euro-International du Béton (CEB) Model Code. Values of γ of 0.026 and $\dot{\varepsilon}_0$ of 3×10^{-6} s^{-1} and 30×10^{-6} s^{-1} in tension and compression respectively are recommended for concrete [30], although $\dot{\varepsilon}_0$ can vary between 1×10^{-6} and 60×10^{-6} s^{-1} in the literature [1, 6, 10]. For asphalt, it has been found that the modulus of elasticity is most sensitive to dynamic loads for $\dot{\varepsilon}_0 \ge 1.7\times10^{-5}$ s^{-1} [31]. For steel,

experimental investigations have shown that the modulus of elasticity remains unchanged at high strain rates [10, 32] but the strain rate has an impact on the steel's yield strength, ultimate tensile strength and strain. In the case of concrete, Yon, et al. [27] use γ values of 0.065 and higher. They assume a 'static' strain rate threshold $\dot{\varepsilon}_0$ of 2.5x10^{-3} s^{-1} based on experimental results, and for a maximum strain rate of 0.24 s^{-1}, they find an increase in the compressive and tensile moduli of concrete of 41% and 60%, respectively. Most of the literature on calibrating γ values for different materials uses experimental data conducted on a cubic specimen under impact loading to create high levels of strain rate at a single point. There are no previous records on how a simply supported beam with high strain rates may respond to a moving load, therefore, a range of γ values is covered here to assess the impact of different degrees of stiffening. In practise, the constitutive model will need to be calibrated on site by taking strain measurements due to the crossing of loads with different magnitudes and at a range of speeds.

The response of the viscoelastic material due to strain rate is incorporated using an equivalent moment of inertia based on the parallel-axis theorem as in Equation (5):

$$I_j(t) = \sum_{k=1}^{N_k} \frac{b_{j,k}(t)d^3}{12} + \left[b_{j,k}(t)d\right](y_k)^2 \tag{5}$$

where $b_{j,k}(t) = b(\frac{E_d(j,k,t)}{E_s})$ is the equivalent width of each strip k in element j at time t. N_k is the total number of strips from the extreme fiber in compression to the extreme fiber in tension. $I_j(t)$ is the equivalent moment of inertia (m^4) of beam element j at time t that provides the stiffness from which the strain rate dependent stiffness matrix of the beam can be attained (Fig. 1).

The process of obtaining the strain rate and equivalent stiffness throughout the beam is repeated in each time step following calculation of the beam response (displacements and strains) by integration of the equation of motion using the Wilson-θ method. Summarizing, all displacements, velocities and accelerations of the beam are initially ('t = 0') assumed to be zero. Following a time increment Δt, the initial elementary stiffness matrices are calculated using Equation (1), and used to assemble the global matrix [K] that will be part of the equation of motion in Fig. 1. Using this equation, the displacements are obtained for the time instant '$t = 0 + \Delta t$', which are converted to strain using Equation (2). Strain rate for '$t = 0 + \Delta t$' is obtained using strain at times '$t = 0 + \Delta t$' and 't = 0' in Equation (3). Once the strain rate is known, the 'dynamic' moduli of elasticity and the equivalent moments of inertia for every element are calculated using Equations (4) and (5) respectively. The latter are used to update the elementary and global stiffness matrices that will be used to calculate new displacements via the equation of motion for the time instant '$t = \Delta t + \Delta t$'. From these

displacements, new strains, strain rates, 'dynamic' moduli of elasticity and equivalent inertias will be obtained and used to update the stiffness matrix in the equation of motion that will provide displacements for the time instant '$t = 2\Delta t + \Delta t$'. This process of calculating displacements -> strain -> strain rates -> 'dynamic' moduli -> equivalent inertias -> updating stiffness matrices illustrated in Fig. 1 is repeated for each subsequent time step. While the full model described by Fig. 1 is implemented in Sections 4 and 5, a simpler model without matrix updating at each point in time is used for the results presented in Sections 2 and 3.

In this section, results are generated using a beam made of a constant modulus of elasticity E_s for comparison purposes. The inputs and outputs have been normalized following recommendations by Frýba [22] to facilitate generalisation of the results to beam structures with other mechanical properties. Two of the normalized input parameters are speed (α) and damping (β) defined in Equations (6) and (7) respectively.

$$\alpha = \frac{L_f}{f_1} \tag{6}$$

where α is the dimensionless speed parameter (renamed frequency ratio by Brady, et al. [33]), L_f is the load frequency given by $\frac{v}{2L}$ (where v is the speed of the moving load (m/s) and L is the span length of the beam (m)) and f_1 is the first natural frequency (Hz) of the beam given by $f_1 = \frac{\pi^2}{L^2}\sqrt{\frac{E_s I}{\mu}}$ (where μ is the mass per unit length (kg/m)).

$$\beta = \frac{\omega_b}{f_1} \tag{7}$$

where β is a dimensionless damping parameter and ω_b is damped natural frequency given by $\frac{\xi\omega_1}{\sqrt{\left(1-\xi^2\right)}}$ (where ξ is the viscous damping factor given by $\frac{c}{2\mu\omega_1}$, being ω_1 and c the circular first natural frequency ($\omega_1 = 2\pi f_1$) and damping coefficient of the beam respectively). Fig. 3(a) illustrates how load frequency (L_f) varies with span length (L) and load speed (v). Fig. 3(b) shows the relationship between load frequency (L_f), beam frequency (f_1) and the speed parameter (α). Fig. 3(a) and Fig. 3(b) provide a quick reference to obtain actual numbers and units that correspond to normalized and dimensionless values in the text

Fig. 3. Simulation parameters involving load speed: (a) Load frequency (Hz), (b) Normalized speed parameter α.

Normalized time, $\overline{t}$, (Equation (8)) indicates the location of the load on the bridge and it goes from 0 (instant at which the load enters the bridge) to 1 (instant at which the load leaves the bridge).

$$\overline{t} = t\frac{v}{L} \tag{8}$$

where t is the time increment (s) and v is the speed of the moving point load (m/s).

Normalized section, $\overline{x}_s$, (Equation (9)) represents the beam location under investigation, i.e., 0, 0.5 and 1 represent the section above the 1st support, the mid-span section and the section above the 2nd support respectively.

$$\overline{x}_s = \frac{x}{L} \tag{9}$$

where x indicates distance (m) from the section under investigation to the left-support.

Strain, $\overline{\varepsilon}$, and displacement, $\overline{u}$, (Equations (10) and (11) respectively) are also normalized by the corresponding maximum static value, which takes place at the mid-span section when the point load is positioned at mid-span.

$$\overline{\varepsilon}\left(x,t\right) = \frac{\varepsilon\left(x,t\right)}{\varepsilon_0} \tag{10}$$

where $\varepsilon\left(x,t\right)$ is the strain at time t and distance x from the left-support due to a dynamic load and ε_0 is the maximum mid-span strain due to a static application of the same load ($\varepsilon_0 = \frac{PLy}{4E_sI}$ for a load of value P and distance y between extreme fiber and neutral axis of the cross-section).

$$\bar{u}\left(x,t\right)=\frac{u\left(x,t\right)}{u_0} \tag{11}$$

where $u\left(x,t\right)$ is the displacement at time t and distance x due to a dynamic load and u_0 is the maximum mid-span displacement due to a static application of the same load ($u_0=\frac{PL^3}{48E_sI}$ for a load of value P).

Table 1 provides the values of the 10 m and 20 m span beams that are investigated. Maximum $\bar{u}$ and maximum $\bar{\varepsilon}$ are plotted versus $\bar{t}$ and $\bar{x}_s$ in Fig. 4 and Fig. 5 for a damping parameter β of 0.02 (i.e., equivalent to a modal damping of 2%, a value within the range typically found in bridges [34]) and three speed parameters: α = 0.1, 0.2 and 0.3. A 'static' stiffness is used in the figures below (i.e., constant modulus E_s). The impact of the use of a dynamic modulus (E_d) and comparisons to the 'static' modulus will be analysed in further sections. The non-dimensional results in Figs. 4 and 5 present a preliminary examination into the impact of the speed of the load on the response of a beam and they are valid for any straight simply supported structure with uniform stiffness and cross-section subjected to a single moving constant load (I.e., these graphs have been generated with the 10 m beam span and validated with the 20 m beam span). Hence, any combination of main beam frequency and load frequency that meet the straight line for α = 0.1 in Fig. 3(b) will produce the same results for normalized displacement and strain observed in Figs. 4 and 5 respectively. For instance, the non-dimensional response of the 10 m beam of Table 1 (f_1 = 10.4 Hz) to a load travelling at 20.8 m/s (load frequency of 1.04 Hz in Fig. 3(a)), is the same as that of the 20 m beam of Table 1 (f_1 = 5 Hz) traversed by a load at 20 m/s (L_f = 0.5 Hz in Fig. 3(a)) or other 10 m bridge with f_1 = 5 Hz traversed by a load at 10 m/s (L_f = 0.5 Hz), given that α is equal to 0.1 in all three cases.

Table 1 Parameters of bridge models

In Fig. 4(a) (α = 0.1), a maximum $\bar{u}$ of 1.06 occurs at $\bar{x}_s$ = 0.52 and $\bar{t}$ = 0.55. In Fig. 4(b) (α = 0.2), a maximum $\bar{u}$ of 1.05 occurs at $\bar{x}_s$ = 0.48 and $\bar{t}$ = 0.35. In Fig. 4(c) (α = 0.3), a maximum $\bar{u}$ of 1.371 takes place at $\bar{x}_s$ = 0.5 (mid-span) and $\bar{t}$ = 0.48. It can be seen how the maximum $\bar{u}$ typically takes place in a section near mid-span, although the location of the load for which the maximum occurs, depends on the speed parameter. Therefore, the impact of the moving load on the response is more noticeable at the highest speed of α = 0.3.

Fig. 4. Normalized displacement versus normalized section and normalized time for a beam with $\beta = 0.02$: a) $\alpha = 0.1$, b) $\alpha = 0.2$ and c) $\alpha = 0.3$

In Fig. 5(a) ($\alpha = 0.1$), a maximum $\bar{\varepsilon}$ of 1.038 occurs at $\bar{x}_s = 0.56$ and $\bar{t} = 0.55$. In Fig. 5(b) ($\alpha = 0.2$), a maximum $\bar{\varepsilon}$ of 1.018 takes place at $\bar{x}_s = 0.36$ and $\bar{t} = 0.35$. In Fig. 5(c) ($\alpha = 0.3$), the maximum $\bar{\varepsilon}$ is 1.291, and takes place at $\bar{x}_s = 0.48$ and $\bar{t} = 0.473$. In contrast to displacements, the critical section holding the maximum response for strain is not always located near mid-span as shown by Fig. 5(b), and the maximum normalized value is generally smaller for strains than for displacements. The latter is attributed to differences in the shapes of the static and dynamic content of the strain and displacement responses. For example, while the static components of the strain and displacement responses at mid-span of a beam are triangular and a 3rd degree polynomial respectively, the dynamic components are sinusoidal. When the static and dynamic components are added together, the total strain response will decrease relatively quicker than the total displacement response as the load starts to move from mid-span towards the supports. Therefore, if the peak of the static component (which takes place when the load is at the measurement location, i.e., it depends on the vehicle speed and the distance from the first support to the measurement location) and a peak of the oscillations due to the dynamic component (which are related to the main frequencies of vibration of the bridge) do not occur at the same time or they are not sufficiently close, the maximum normalized strain will tend to be of a smaller magnitude than the maximum normalized displacement.

Fig. 5. Normalized strain at the bottom fibbers versus normalized section and normalized time for a beam with $\beta = 0.02$: a) $\alpha = 0.1$, b) $\alpha = 0.2$ and c) $\alpha = 0.3$

Results for normalised displacement in Fig. 4 indicate that the maximum occurs at a section near mid-span ($\bar{x}_s = 0.5$), but it does not necessarily take place when the load is located at mid-span which would correspond to $\bar{t} = 0.5$. The maximum indeed takes place close to mid-span for $\alpha = 0.1$ and $\alpha = 0.3$, but this is not the case for $\alpha = 0.2$ when peak $\bar{u}$ are found when the load is at quarter span ($\bar{t} = 0.35$) and three-quarter span ($\bar{t} = 0.66$). In the case of normalised strain, the maximum occurs again when the load is close to mid-span for speeds of $\alpha = 0.1$ and $\alpha = 0.3$, but for $\alpha = 0.2$, peak $\bar{\varepsilon}$ appear when the load is at quarter span ($\bar{t} = 0.35$) at a section of $\bar{x}_s = 0.36$ and when the load is at three quarter span ($\bar{t} = 0.65$) at a section of $\bar{x}_s = 0.66$. These figures give an indication of those critical beam sections holding the highest normalized responses and the critical speeds at which they occur. Largest gradients in the contour plot of Fig. 4 also allow identifying those beam sections more sensitive to a strain rate dependant material and as a result, more prone to disparities with the results shown here for $\gamma = 0$.

Equation (3) is used to obtain a preliminary estimate of the strain rates $\dot{\varepsilon}$ (or variation of strain with time) that may develop at each beam section. For this purpose, it is first necessary to convert the normalized strain of Fig. 5 into strain using Equation (10). The latter requires assuming a beam section, which in this case, it is a rectangular shape of depth 0.6 m (i.e., neutral axis at 0.3 m from the extreme fibers of the section). So, Figs. 6, 7 and 8 show the normalised strain rate $\left(\frac{\dot{\varepsilon}}{\dot{\varepsilon}_0}\right)$ (where $\dot{\varepsilon}_0 = 30\times10^{-6}\ \mathrm{s}^{-1}$ is the strain rate at which the load is deemed to be 'static') of the top fiber (in compression) of a rectangular cross-section versus normalised time $\bar{t}$ and section $\bar{x}_s$ for different α values. Three vertical (fixed sections) and three horizontal (fixed points in time) sections through the contour plot are provided with each figure to illustrate how the normalized strain rates vary with time at a given section, and also how they change with the section location at a given point in time. If the beam section was made of a strain-rate dependant material such as concrete, those normalized values of strain rate above 1 would be indicative of potential changes in modulus that can lead to total responses smaller than predicted by Figs. 4 and 5. For α = 0.1, a maximum positive normalized strain rate of 3.2 occurs at $\bar{x}_s$ = 0.28 and $\bar{t}$ = 0.081 (Fig. 6). For α = 0.2, the maximum positive normalized strain rate is 6.6 and it occurs at $\bar{x}_s$ = 0.26 and $\bar{t}$ = 0.162 (Fig. 7). Finally, for α = 0.3, the maximum positive normalized strain rate is 10.2, and again, it takes place at $\bar{x}_s$ = 0.28 and $\bar{t}$ = 0.24 (Fig. 8). High strain rates occur all throughout the span length, although they tend to be positive (increase in strain with time) in the first half, and negative (decrease in strain with time) in the 2nd half. The impact of speed on strain rate is more significant than on strain or displacement responses. As the speed parameter is increased so is the maximum absolute strain rate, i.e., by 100% (doubled) from α = 0.1 to α = 0.2, and by 54% from α = 0.2 to α = 0.3.

Fig. 6. a) Normalized strain rate versus normalized section and normalized time for a beam with β = 0.02 and α = 0.1, b) Vertical sections (A =0.25, B =0.5, C =0.75), c) Horizontal sections (D =0.25, E =0.5, F =0.75)

Fig. 7. a) Normalized strain rate versus normalized section and normalized time for a beam with β = 0.02 and α = 0.2, b) Vertical sections (A =0.25, B =0.5, C =0.75), c) Horizontal sections (D =0.25, E =0.5, F =0.75)

Fig. 8. a) Normalized strain rate versus normalized section and normalized time for a beam with β = 0.02 and α = 0.3, b) Vertical sections (A =0.25, B =0.5, C =0.75), c) Horizontal sections (D =0.25, E =0.5, F =0.75)

The maximum strain rate at $\bar{x}_s$ = 0.28 for α = 0.3 (Fig. 8) can be explained as a result of the strain rate due to the dynamic component (of a sinusoidal nature) reaching a peak together

with the strain rate due to the static component for that section. The strain rate is essentially the slope of the strain curve and locations with the highest strain rate (Figs. 6, 7 and 8) don't necessarily correspond to locations with the highest strain (Fig. 5).

3- Material Properties

Equation (4) can be visualized in Fig. 9 for a range of materials with different γ values. The strain rate variation (horizontal axis) will depend on the load, its speed and the flexibility of the structure. For strain rates between -30×10^{-6} s^{-1} and 30×10^{-6} s^{-1} (typical of concrete in compression), the modular ratio is assumed to be 1 (i.e., the load is being applied statically) following recommendations by CEB- FIP [30]. The level of increase in the modulus of elasticity above 30×10^{-6} s^{-1} (or below -30×10^{-6} s^{-1}) is directly related to γ (i.e., modular ratios E_d/E_s of 1.016 and 1.065 are found for γ = 0.013 and γ = 0.052 respectively at 10^{-4} s^{-1}). The rate of increase in the modular ratio is lower for higher strain rates. For example, the modulus of a material with a γ value of 0.026 increases by 1.8% when strain rate rises from 30×10^{-6} s^{-1} to 60×10^{-6} s^{-1}, but only by 1.1% when rising from 60×10^{-6} s^{-1} to 90×10^{-6} s^{-1}. For a brittle material such as concrete, the static strain rate threshold ($\dot{\varepsilon}_0$) in tension is lower than in compression and as a result, modular ratio in tension will be larger than 1 across a wider range than shown in Fig. 9.

Fig. 9. Ratio of 'dynamic' to'static' modulus of elasticity versus strain rate for different γ values

Fig. 10(a) shows the variation of strain rate together with the variation in modulus versus time for the compression of the top fiber of the mid-span section when a 100 kN load is travelling at 25 m/s (α = 0.12) on a 10 m span bridge (cross-section of 12 m width and 0.6 m depth). In this figure, the strain rate is calculated at mid-span via Equation (3) and used to obtain the 'dynamic' modulus E_d via Equation (4) (assuming a γ of 0.026 and $\dot{\varepsilon}_0$ values of 30×10^{-6} and 3×10^{-6} s^{-1} in compression and tension respectively [30]) at each time step. Strain and E_d values are stored for the next time step and the process is repeated as described in section 2.

For this particular speed, the modulus reaches the static value (35×10^9 N/m^2) at different intervals approximately centred about 0.1 s, 0.19 s, 0.24 s and 0.34 s after the load enters the bridge. Fig. 10(b) compares the variation of modulus at the bottom fiber of the section (in tension) to that at the top (in compression), being the first more significant due to a lower $\dot{\varepsilon}_0$. Maximum variation of modulus of 3.4% and 10% with respect to the 'static' value are obtained in compression and tension respectively, approximately 0.05 s after the load enters

the bridge. Of course, the situation of Fig. 10(b) is unrealistic given that tensile stresses will typically be resisted by steel instead of concrete. For this reason, analysis in further sections will conservatively assume that changes in modulus only occur in the compression side of the section.

Fig. 10. Variation of modulus with time at mid-span element for $\gamma = 0.026$: (a) comparison of modulus and strain rate in compression, (b) comparison of modulus in tension and compression

In Fig. 10(a), there is a positive strain rate (increase in strain) up to the point when the load is on mid-span and negative (decrease in strain) as the load moves away from mid-span. When the load is located at the mid-span section, the strain rate is relatively small. This abrupt change in strain rate is revealed as a distinct line at 45° in Figs. 6, 7 and 8 and it is the trigger for the sudden change in 'dynamic' modulus of Fig. 10(b) as the load crosses mid-span. It must be pointed that the theoretical variations in strain rate shown in this paper are relatively smooth, and in reality, they will be affected by vehicle-road-bridge dynamic interaction.

Figs. 11-13 illustrate the ratio of E_d to E_s, versus normalized time and normalized section. The values in the figure are obtained using Equation (4), where γ and $\dot{\varepsilon}_0$ have been assumed to be 0.026 and 30×10^{-6} s^{-1} respectively in the compression side, and the strain rate has been obtained from Figs. 6-8. The latter is a simplification given that Figs. 6-8 neglect the influence of changes in moduli throughout the beam length and depth with time on strain rate, and they are intended here merely to serve as a preliminary evaluation of how much the moduli may vary. Full simulations taking into account the time-varying nature of the stiffness matrix (Fig. 1) and also bridge specific properties are used to derive the results in Sections 4, 5 and 6. As expected, the patterns of Fig. 6-8 and Figs. 11-13 are similar, particularly at the peak locations. When the speed parameter, α, is increased from 0.1 (Fig. 11) to 0.2 (Fig. 12), the maximum 'dynamic' modulus, E_d, only increases slightly from 1.03 (for the 10 m bridge in Table 1, it corresponds to a speed of 20.8 m/s, producing a maximum modulus in a section at 2.8 m from left-support and 0.041 s after the load has entered the bridge) to 1.05 (for the 10 m bridge, it corresponds to a speed of 41.6 m/s, producing a maximum modular ratio in a section at 2.8 m and 0.038 s after the load has entered the bridge) times the 'static' modulus E_s. For α = 0.3 (Fig. 13), changes are more significant and the maximum modular ratio reaches 1.062 (that in the case of the 10 m bridge, it corresponds to a speed of 62.4 m/s leading to a maximum modular ratio in a section at 2.8 m and 0.042 s after the load has entered the bridge).

Fig. 11. a) Modular ratio versus normalized time and normalized section, β = 0.02, γ = 0.026 and α = 0.1, b) Vertical sections (A =0.25, B =0.5, C =0.75), c) Horizontal sections (D =0.25, E =0.5, F =0.75)

Fig. 12. a) Modular ratio versus normalized time and normalized section, β = 0.02, γ = 0.026 and α = 0.2, b) Vertical sections (A =0.25, B =0.5, C =0.75), c) Horizontal sections (D =0.25, E =0.5, F =0.75)

Fig. 13. Modular ratio versus normalized time and normalized section, β = 0.02, γ = 0.026 and α = 0.3, b) Vertical sections (A =0.25, B =0.5, C =0.75), c) Horizontal sections (D =0.25, E =0.5, F =0.75)

The depth of the beam also plays an important role regarding what fibers will experience a strain rate above the static threshold and as a result, contribute to a change in the neutral axis and in the equivalent section stiffness (= equivalent modulus of elasticity multiplied by second moment of area). Fig. 14 shows the stiffness ratio versus strain rate for a rectangular section with γ = 0.026 in the compression side (γ = 0 in the tension side). Here, stiffness ratio is the ratio of equivalent section stiffness (based on the variation of E_d throughout the depth) to 'static' stiffness ($=E_sI$). Larger beam depths lead to higher increases in the equivalent section stiffness. Once the static threshold is exceeded, the equivalent stiffness increases very rapidly up to a strain rate of 0.5×10^{-3} s^{-1} after which the increments become more moderate.

Fig. 14. Stiffness ratio versus strain rate for γ = 0.026 and different section depths.

4- Effect on Displacements and Strains

Displacement and strain responses in Fig. 4 and Fig. 5 have been generated based on the assumption that the modulus of the beam and the global stiffness matrix of the model remain constant with time. In order to analyse the effect of a strain-rate dependant modulus and global stiffness matrix, the entire beam is discretized into 50 finite beam elements. Each elementary beam experiences a strain rate that results into a distribution of moduli of elasticity along the structure. The calculation of the modulus of elasticity for a given beam element is somewhat tedious (Section 2), as strain and strain rate varies for different depths of the beam section. Given that the behaviour in compression and tension are different, the

neutral axis can change at different points in time. As a result of applying Equation (4), different moduli of elasticity are found at different depths of a section if the 'static' strain rate is exceeded. The latter requires the determination of an equivalent modulus of elasticity and stiffness (as shown in Fig. 14 for sections of different depths).

A typical section for a short-span bridge is investigated here. The dimensions of the beam are 10 (long) ×12 (wide) × 0.6 (deep) m. The material is assumed to have a 'static' modulus (E_s) and 'static' strain rate for compression ($\dot{\varepsilon}_0$) of 35×10^9 N/m^2 and 30×10^{-6} s^{-1} respectively (the tensile side is conservatively assumed to be unaltered by the strain rate). The density μ is 2400 kg/m^3, the first natural frequency f_1 is 10.38 Hz, and a 2% damping ratio is adopted (β = 0.02). The discretized finite element model is made of 50 elementary beams 0.2 m long each (L_j = 0.2 m) and the depth d of each beam strip k is adopted to be 0.003 m (Fig. 2). Unless otherwise specified, the properties of this beam model are maintained in the results of the remaining sections of the paper. Figs. 15 and 16 show the $\bar{u}$ and $\bar{\varepsilon}$ respectively versus $\bar{t}$ and $\bar{x}_s$ for α = 0.2 (equivalent to a load travelling at 41.6 m/s for the bridge under investigation) and α = 0.3 (equivalent to a load travelling at 62.4 m/s) when traversed by a load of 100 kN. For α = 0.2 (Fig. 15(a)), the maximum $\bar{u}$ is 1.0012 (taking place at $\bar{x}_s$ = 0.55 (5.5 m) and $\bar{t}$ = 0.644 (0.155 s after the load enters the bridge)), which is 5% less than using γ = 0 (Fig. 4(b)). For α = 0.3 (Fig. 15(b)), the maximum $\bar{u}$ is 1.283 (at $\bar{x}_s$ = 0.5 (5 m) and $\bar{t}$ = 0.464 (0.074 s)) with a 7% reduction compared to γ = 0 (Fig. 4(c)). Similar patterns are found for higher loads, although strain and strain rate will be larger, and as a result, the modulus and the normalized response will be affected to a greater extent. For example, a maximum $\bar{u}$ of 1.226 (at $\bar{x}_s$ = 0.5 and $\bar{t}$ = 0.46), which represents a 12% reduction compared to Fig. 4(c), is obtained for a 500 kN load and α = 0.3 (62.4 m/s).

Fig. 15. Normalized displacement versus normalized time and normalized section for β = 0.02 and γ = 0.026 at speed parameter of a) α = 0.2 and b) α = 0.3

The percentage reduction in maximum normalized response comparing γ = 0.026 to γ = 0 is slightly smaller for strain than for displacement, in part due to the fact that maximum $\bar{u}$ for γ = 0 is larger than maximum $\bar{\varepsilon}$ for γ = 0. For α = 0.2 (Fig. 16(a)), the maximum $\bar{\varepsilon}$ is 1 (at $\bar{x}_s$ = 0.6 (6 m) and $\bar{t}$ = 0.62 (0.144 s) with 1.8% reduction compared to γ = 0 (Fig. 5(b)). For α = 0.3 (Fig. 16(b)), the maximum value of normalized strain is 1.228 (at $\bar{x}_s$ = 0.44 (4.4 m) and $\bar{t}$ = 0.473 (0.076 s)) which is 5.15% less than for γ = 0 (Fig. 5(c)).

Fig. 16. Normalized strain versus normalized time and normalized section for β = 0.02 and γ = 0.026 at speed parameter of a) α = 0.2 and b) α = 0.3

Fig. 17 shows the normalized displacement at mid-span using two types of beam material (γ = 0 and γ = 0.026) and a load of 100 kN with three speed parameters (α = 0.1, 0.2 and 0.3 which correspond to 20.8, 41.6 m/s, and 62.4 m/s respectively for a 10 m bridge – Fig. 3). While it is unlikely to reach speeds of 62.4 m/s in highway bridges, speeds of up to 83 m/s can be achieved in railway bridges [35]. For α = 0.1, the difference between both materials is small due to the relatively low strain rate as well as the assumption that the section material is only varying stiffness in the compression side. When α = 0.3, the maximum $\overline{u}$ decreases from 1.371 for a perfectly elastic material (γ = 0) to 1.283 for a viscoelastic material with γ = 0.026.

Fig. 17. Normalized displacement at mid-span section due to a 100 kN load with α = 0.1, 0.2 and 0.3, β = 0.02 and two materials: γ = 0.026 (dotted line) and (γ = 0) (solid line)

Similar results are obtained when calculating the normalized strain for different speed parameters as shown by Fig. 18. For a small load of 100 kN, a high speed parameter α is needed to notice significant differences in the mid-span strain between materials with γ = 0 and γ = 0.026.

Fig. 18. Normalized strain at mid-span section due to a 100 kN load with α = 0.1, 0.2 and 0.3, β = 0.02 and two materials: γ = 0.026 (dotted line) and (γ = 0) (solid line)

In addition to γ, the 'static' strain rate threshold, $\dot{\varepsilon}_0$, has a significant influence on the response. For concrete, the 'static' strain range is between 5×10^{-6} and 50×10^{-6} s^{-1} above which the strain rate is quasi-static and dynamic respectively according to Bischoff and Perry [2]. Shkolnik [1] utilises a $\dot{\varepsilon}_0$ of 30×10^{-6} s^{-1} (also suggested by the CEB-FIP model) to graph the stress-strain curve at high strain rates and finds considerable changes in the modulus of elasticity and strength of concrete in both tension and compression. Having said that, the strain rates used by Shkolnik are very high (in the range of 0.1 s^{-1} and applicable to impact load) compared to the strain rates used in this moving load investigation (typically between 30×10^{-6} and 2×10^{-4} s^{-1}). Fig. 19 shows the displacement that would result from using different $\dot{\varepsilon}_0$ values. It can be seen how lowering $\dot{\varepsilon}_0$ increases the stiffness considerably, i.e., a $\dot{\varepsilon}_0$ of

1×10^{-6} s^{-1} reduces the maximum displacement by almost 10% with respect to a $\dot{\varepsilon}_0$ of 30×10^{-6} s^{-1}.

Fig. 19. Normalized displacement at mid-span using different $\dot{\varepsilon}_0$ values for α = 0.1, β = 0.02, and γ = 0.026.

5- Influence of Load Magnitude and Speed on the Response

An increase in load from 100 to 500 kN for a material with γ = 0.026 has a significant impact on the mid-span normalized displacement, even for a relatively low speed parameter of α = 0.1 (Fig. 20(a)). Strain rate and stiffness increases with load and as a result, the maximum $\overline{u}$ for 500 kN is 7% lower than for 100 kN. A similar effect can be achieved with only 200 kN but increasing α to 0.3 (Fig. 20(b)). In the latter, the maximum $\overline{u}$ decreases from 1.28 for 100 kN (Fig. 17) to 1.26 for 200 kN. Using α = 0.3, the percentage difference between maximum $\overline{u}$ considering γ = 0 and γ = 0.026 is 8.8% for 200 kN and 6.8% for 100 kN. α values of 0.1 and 0.2 lead to percentage differences in maximum $\overline{u}$ of 6.3% and 5.1% respectively for the 100 kN load, and 8.3% and 6.9% respectively for 200 kN. These results indicate that changes in displacement and strain using a 'dynamic' modulus are relatively small compared to using a 'static' modulus, although they can become more important as speed and magnitude of load is increased. Hence, the effect of a viscoelastic material will be more significant when dealing with critical loading scenarios that in bridges typically consist of a number of heavy vehicles/trains crossing the bridge simultaneously.

Fig. 20. Normalized displacement at mid-span with β = 0.02 traversed by loads of: (a) 100 and 500 kN at α = 0.1, with γ = 0.026 (b) 200 kN at α = 0.1, α = 0.2, and α = 0.3 and two beam materials: γ = 0 (solid line) and γ = 0.026 (dotted line)

The use of a dynamic amplification factor (DAF) is a popular way of quantifying the dynamic increment in the total response to a moving load with respect to the static component. DAF is typically defined as the ratio of the maximum total response to the maximum static response at a given bridge section for a given load and response [33]. This definition of DAF corresponds to the maximum normalized response shown in Figs. 4 and 5 for displacement and strain respectively for the case of a moving point load. However, it must be noted that although maximum static response due to a point load always corresponds to the mid-span section, the latter may not hold true for the maximum total response. For this reason, some authors [36] prefer to use the concept of full dynamic amplification factor (FDAF), given by the maximum total response of all beam sections divided by the maximum

static response at a specific section, typically mid-span. Therefore, FDAF ≥ maximum mid-span normalized response.

The impact of γ on FDAF of mid-span displacement can be visualized versus speed parameter α in Fig. 21. Here, the moving load is 100 kN. The numerator and denominator that define FDAF are given by the maximum total response and maximum static response respectively. As illustrated earlier, an increase in speed leads to a rise in stiffness, being the latter more significant the higher the γ. If γ = 0, numerator and denominator are based on the same modulus of elasticity (E_s), but if $\gamma \neq 0$, the numerator is based on a 'dynamic' modulus of elasticity (E_d) while the denominator of FDAF remains to be based on E_s. Therefore, the higher the γ, the lower the FDAF. For instance, a speed of 20.8 m/s ($\alpha \cong 0.1$) leads to DAFs of 1.06, 1.02 and 0.97 for materials with γ = 0, 0.026 and 0.052 respectively. Doubling the speed to 41.6 m/s ($\alpha \cong 0.2$) results in FDAFs of 1.06 for γ = 0, 1.03 for γ = 0.026 and 0.99 for γ = 0.05. At 80 m/s ($\alpha \cong 0.4$), these differences in FDAF become more significant, i.e., 1.54 for γ = 0, 1.44 for γ = 0.026, and 1.34 for γ = 0.052. The reader needs to be mindful that these results are based on theoretical simulations of a moving constant load over a 1-D simply supported beam where the beam section has been assumed to be rectangular and made of a homogenous material that obeys the constitutive Equation (4) in the compression side. These simulations have ignored the effect of strain rate in the tensile side, the influence of reinforcement at the bottom of the section, vehicle-bridge interaction and road irregularities. In practise, a calibrated finite element model based on specific constitutive equations developed for the bridge under investigation, will be needed to judge the degree of stiffening of the structure under the moving loads and their potential impact on FDAF. Having said this, Figs. 21 and 22 show that the dynamic component of the total response can be reduced very significantly for a strain-rate dependant material, and that a high level assessment taking into account viscoelastic properties could save a bridge from unnecessary intervention.

Fig. 21. FDAF of displacement at mid-span for different speed parameters and γ value

Two bridge spans of 10 m and 20 m with cross-sectional properties provided in Table 1 [37] are tested for three values of γ under different load magnitudes (100 kN and 500 kN). Fig. 22 shows the pattern of FDAF of mid-span strain versus speed. For $\alpha \leq 0.4$, maximum FDAF of strain in Fig. 22(a) is found to be 8% less than FDAF of displacement in Fig. 22 for γ = 0. Different γ values produce patterns of FDAF which have similar characteristics in terms of pattern and overall shape, but typically lower FDAF values are obtained for higher γ, most noticeably at the location of the peaks. It can also be seen that the FDAF peaks for $\gamma \neq 0$ take place at a higher critical speed than for $\gamma = 0$. The FDAFs in the 10 m bridge

(Fig. 22(a)) appear to be more sensitive to γ than the FDAFs in the 20 m bridge (Fig. 22(b)) due to their cross-sectional properties relative to the applied load and the strain rate that develops. For a material with $\gamma \neq 0$, the higher the load (100 kN in Fig. 22(b) and 500 kN in Fig. 22(c)), the more significant decrease in FDAF with respect to $\gamma = 0$ (As opposed to a material with $\gamma = 0$, where the FDAF pattern will not vary with the magnitude of the applied load). The analysis has revealed significant differences in the maximum FDAF for speeds below 80 m/s depending on the material: 1.42 ($\gamma = 0$) and 1.37 ($\gamma = 0.026$) for a 10 m bridge subjected to 100 kN, 1.44 ($\gamma = 0$) and 1.39 ($\gamma = 0.026$) for a 20 m bridge subjected to 100 kN, and 1.44 ($\gamma = 0$) and 1.358 ($\gamma = 0.026$) for a 20 m bridge subjected to 500 kN.

Fig. 22. FDAF of mid-span strain versus load speed; (a) 10 m span and 100 kN load, (b) 20 m span and 100 kN load, (c) 20 m span and 500 kN load; $\gamma = 0$ (solid line), $\gamma = 0.013$ (dashed line), $\gamma = 0.026$ (dotted line), $\gamma = 0.052$ (dotted line)

6- Conclusions

This paper has investigated the response of a beam made of a viscoelastic material to a moving load. The ratio between 'dynamic' and 'static' moduli has been assumed to be related to strain rate through a power parameter denoted γ. Below a strain rate between 3×10^{-6} and 30×10^{-6} s^{-1}, the modulus of elasticity is assumed to be 'static', but once this threshold is exceeded, the 'dynamic' modulus of elasticity increases with higher strain rates. This increment depends on the selected 'static' threshold and the parameter γ that measures the degree of stiffening of the material. Results have shown how strain rate and modulus vary throughout the beam length as the load moves across the structure. For a mid-span section, the largest changes in modulus of elasticity have been observed to take place approximately when the moving load is over the section. Variations in the strain and displacement response have been typically small (< 5%) for moderate loads and speeds. However, higher magnitudes and speeds of the load, and higher γ values have led to higher strain rates and more significant changes in the stiffness distribution throughout the beam. The latter could take place within modern scenarios consisting of heavy loads travelling at high speed such as high-speed trains on slender railway concrete bridges. It has been shown how changes in moduli of elasticity will affect the main frequency of the beam, that will become higher the larger the α and γ values. FDAF has proved to be particularly sensitive to γ. For instance, the mid-span strain has experienced a peak FDAF of 1.44 in a 20 m span for $\gamma = 0$, but it has been reduced to 1.39 for $\gamma = 0.026$ when traversed by a 100 kN load (being γ considered only on the compression side). This peak FDAF has been further reduced to 1.36 for $\gamma = 0.026$ and a 500 kN load. Absolute changes in FDAF have shown to be more significant for the displacement response (from 1.54 ($\gamma = 0$) to 1.44 ($\gamma = 0.026$)) than for the strain

response (from 1.42 (γ = 0) to 1.37 (γ = 0.026)) when a 10 m span has been traversed by a 100 kN. It is likely that the constitutive equations and 'static' strain rate thresholds assumed here will differ from those fitting a particular concrete structure depending on the shape of the cross-section, amount of reinforcement, concrete and steel specifications, etc. Further research and experimental data is needed to accurately characterise the response of a specific cross-section to a moving load.

References

[1] I. E. Shkolnik, "Influence of high strain rates on stress–strain relationship, strength and elastic modulus of concrete," *Cement and Concrete Composites,* vol. 30, pp. 1000-1012, 2008.

[2] P. Bischoff and S. Perry, "Compressive behaviour of concrete at high strain rates," *Materials and Structures,* vol. 24, pp. 425-450, 1991.

[3] S. Jerath and M. M. Shibani, "Dynamic Modulus for Reinforced Concrete Beams," *Journal of Structural Engineering,* vol. 110, pp. 1405-1410, 1984.

[4] S. Kolias and R. Williams, "Relationships between the static and the dynamic moduli of elasticity in cement stabilised materials," *Materials and Structures,* vol. 13, pp. 99-107, 1980.

[5] D. Grote, S. Park, and M. Zhou, "Dynamic behavior of concrete at high strain rates and pressures: I. experimental characterization," *International Journal of Impact Engineering,* vol. 25, pp. 869-886, 2001.

[6] D. Yan and G. Lin, "Dynamic properties of concrete in direct tension," *Cement and concrete research,* vol. 36, pp. 1371-1378, 2006.

[7] J. Norambuena-Contreras, D. Castro-Fresno, A. Vega-Zamanillo, M. Celaya, and I. Lombillo-Vozmediano, "Dynamic modulus of asphalt mixture by ultrasonic direct test," *NDT & E International,* vol. 43, pp. 629-634, 10// 2010.

[8] D. Asprone, R. Frascadore, M. Di Ludovico, A. Prota, and G. Manfredi, "Influence of strain rate on the seismic response of RC structures," *Engineering Structures,* vol. 35, pp. 29-36, 2012.

[9] T. J. Memory, D. P. Thambiratnam, and G. H. Brameld, "Free vibration analysis of bridges," *Engineering Structures,* vol. 17, pp. 705-713, 1995.

[10] M. Wakabayashi, T. Nakamura, S. Iway, and Y. Hayashi, "Effects of strain rate on the behavior of structural members," *Proc. 8th World Conference on Earthquake Engineering,* vol. 4, pp. 491-498, 1994.

[11] B. S. I. BSI, "The Structural Use of Concrete," in *CP110-Part 1*, ed. London: British Standards Online, 1972.

[12] J. Willis, "Correlation of calculated and measured dynamic behaviour of bridges," 1977.

[13] F. D. Lydon and R. V. Balendran, "Some observations on elastic properties of plain concrete," *Cement and Concrete Research,* vol. 16, pp. 314-324, 5// 1986.

[14] B. S. I. BSI, "Structural use of concrete. Code of practice for special circumstances," vol. BS 8110-2:1985, ed: BSI, 1985.

[15] A. M. Neville, *Properties of concrete*: John Wiley & Sons, 1996.

[16] M. Şimşek, T. Kocatürk, and Ş. D. Akbaş, "Dynamic behavior of an axially functionally graded beam under action of a moving harmonic load," *Composite Structures,* vol. 94, pp. 2358-2364, 7// 2012.
[17] J.-S. Wu and L.-K. Chiang, "Out-of-plane responses of a circular curved Timoshenko beam due to a moving load," *International Journal of Solids and Structures,* vol. 40, pp. 7425-7448, 12// 2003.
[18] H. Xu and W. L. Li, "Dynamic behavior of multi-span bridges under moving loads with focusing on the effect of the coupling conditions between spans," *Journal of Sound and Vibration,* vol. 312, pp. 736-753, 5/20/ 2008.
[19] P. N. Saavedra and L. A. Cuitiño, "Crack detection and vibration behavior of cracked beams," *Computers & Structures,* vol. 79, pp. 1451-1459, 6// 2001.
[20] A. González and D. Hester, "An investigation into the acceleration response of a damaged beam-type structure to a moving force," *Journal of Sound and Vibration,* vol. 332, pp. 3201-3217, 2013.
[21] H. P. Lee, "Transverse vibration of a Timoshenko beam acted on by an accelerating mass," *Applied Acoustics,* vol. 47, pp. 319-330, 4// 1996.
[22] L. Frýba, *Vibration of solids and structures under moving loads*: Thomas Telford, 1999.
[23] Y. B. Yang, J. Yau, and Y. Wu, *Vehicle-bridge interaction dynamics: with applications to high-speed railways*: World Scientific Pub Co Inc, 2004.
[24] A. González, "Vehicle-bridge dynamic interaction using finite element modelling," *Finite element analysis,* pp. 637-662, 2010.
[25] H. Ouyang, "Moving-load dynamic problems: A tutorial (with a brief overview)," *Mechanical Systems and Signal Processing,* vol. 25, pp. 2039-2060, 8// 2011.
[26] D. Stancioiu, H. Ouyang, J. E. Mottershead, and S. James, "Experimental investigations of a multi-span flexible structure subjected to moving masses," *Journal of Sound and Vibration,* vol. 330, pp. 2004-2016, 4/25/ 2011.
[27] J. H. Yon, N. M. Hawkins, and A. S. Kobayashi, "Strain-rate sensitivity of concrete mechanical properties," *ACI Materials Journal,* vol. 89, 1992.
[28] A. González, *Development of a Bridge Weigh-In-Motion System: A technology to convert the bridge response to the passage of traffic into data on vehicle configurations, speeds, times of travel and weights*. Germany: LAP Lambert Academic Publishing AG & Co. KG, 2010.
[29] Aied. H and Gonzalez. A, "The Effect of Strain Rate on the Total Response of a Structure subject to a Moving Load," *The Thirteenth International Conference on Civil, Structural and Environmental Engineering Computing, CC2011,* pp. Paper no-CC123, 06-SEP-2011 - 09-SEP-2011 2011.
[30] R. E. Rowe and R. Walther, "CEB-FIP Model Code 1990," in *No. 203*, B. D'Information, Ed., ed. lausanne switzerland: Comite Euro-International du Beton, 1991.
[31] D. Katsuki and M. Gutierrez, "Viscoelastic damage model for asphalt concrete," *Acta Geotechnica,* vol. 6, pp. 231-241, 2011/12/01 2011.
[32] C. H. Norris, R. J. Hansen, M. J. Holley, J. M. Biggs, S. Namyet, and J. K. Minami, *Structural design for dynamic loads*: McGraw-Hill New York, 1959.
[33] S. P. Brady, E. J. O'Brien, and A. Znidarič, "Effect of Vehicle Velocity on the Dynamic Amplification of a Vehicle Crossing a Simply Supported Bridge," *Journal of Bridge Engineering,* vol. 11, pp. 241-249, 2006.
[34] R. Cantieni, "Dynamic load testing of highway bridges," *Transportation research record.,* vol. 2, 1984.

[35] H. Xia, N. Zhang, and G. De Roeck, "Dynamic analysis of high speed railway bridge under articulated trains," *Computers & Structures,* vol. 81, pp. 2467-2478, 10// 2003.
[36] D. Cantero, A. González, and E. J. OBrien, "Maximum dynamic stress on bridges traversed by moving loads," *Proceedings of the ICE-Bridge Engineering Journal,* vol. 162, pp. 75-85, 2009.
[37] A. González, D. Cantero, and E. OBrien, "Dynamic increment for shear force due to heavy vehicles crossing a highway bridge," *Computers & Structures,* vol. 89, pp. 2261-2272, 2011.

Table_1
Click here to download Table: Table 1.docx

Type (cross-section)	Length (m)	Mass per unit length (kg/m)	Second moment of inertia (m^4)	1st natural frequency (Hz)	Depth (m)
Rectangular	10	17280	0.216	10.4	0.60
Rectangular	20	33267	1.541	5.0	1.16

Table 1 Parameters of bridge models.

Figure_1
Click here to download Figure: Figure 1.docx

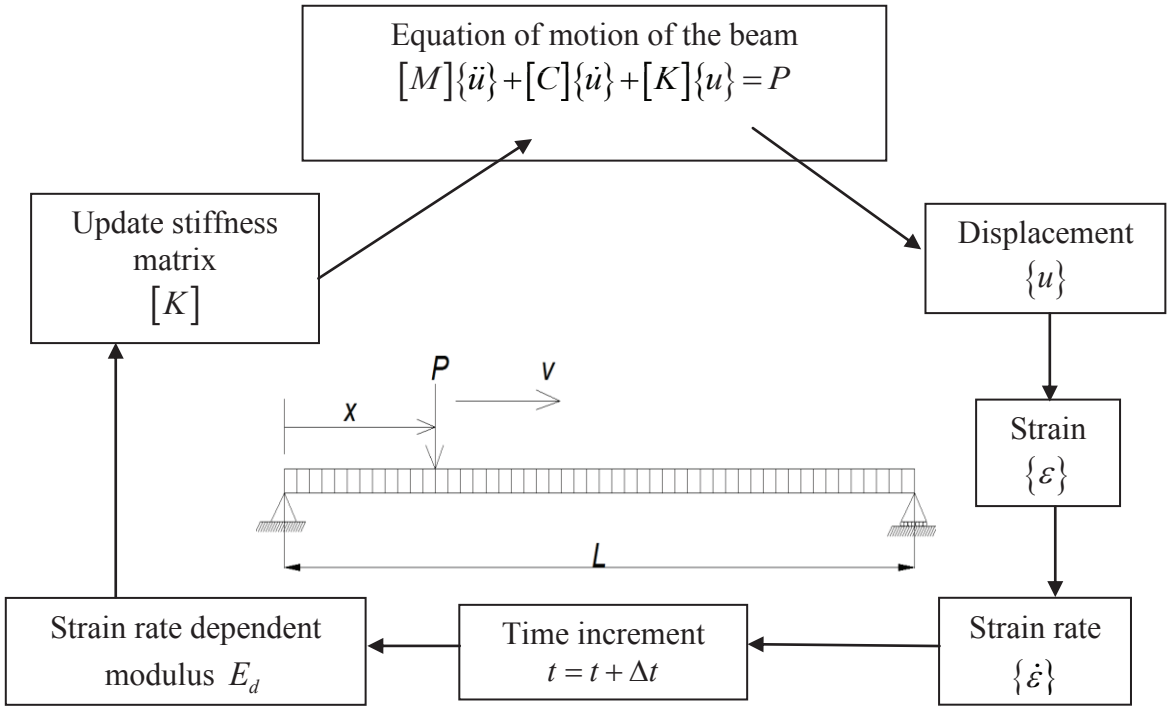

Fig. 1. Simulation model

Figure_2
Click here to download Figure: Figure 2.docx

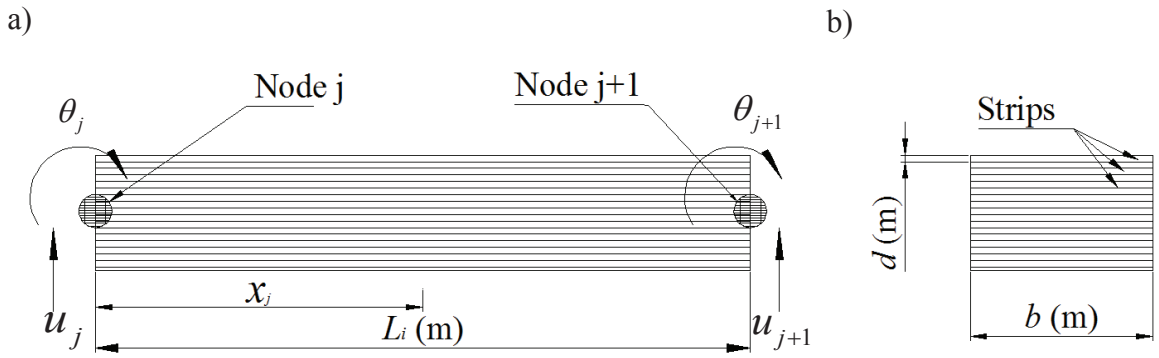

Fig. 2. Elementary beam element: a) Elevation, b) cross-section

Figure_3
Click here to download Figure: Figure 3.docx

a) b)

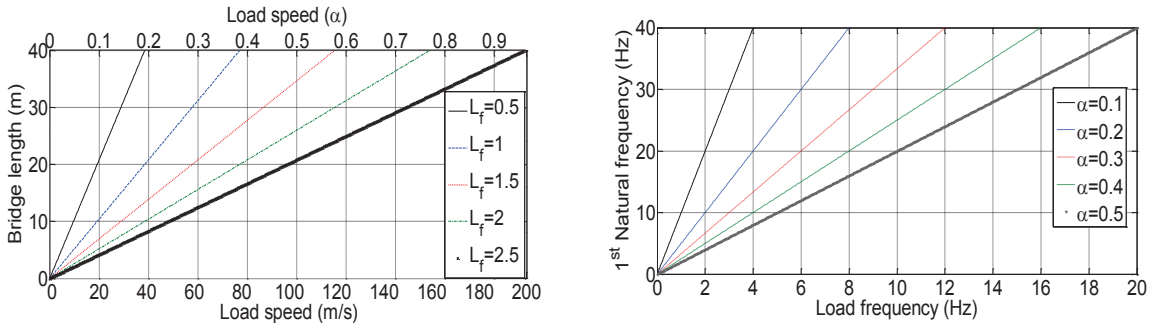

Fig. 3. Simulation parameters involving load speed: (a) Load frequency (Hz), (b) Normalized speed parameter α.

Figure_4
Click here to download Figure: Figure 4.docx

a)

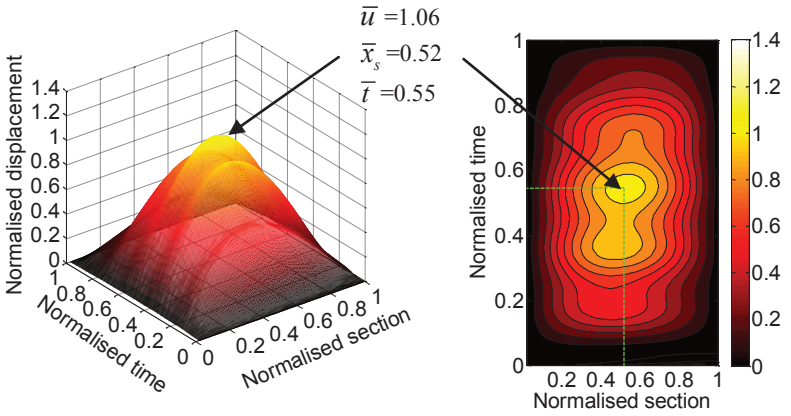

b)

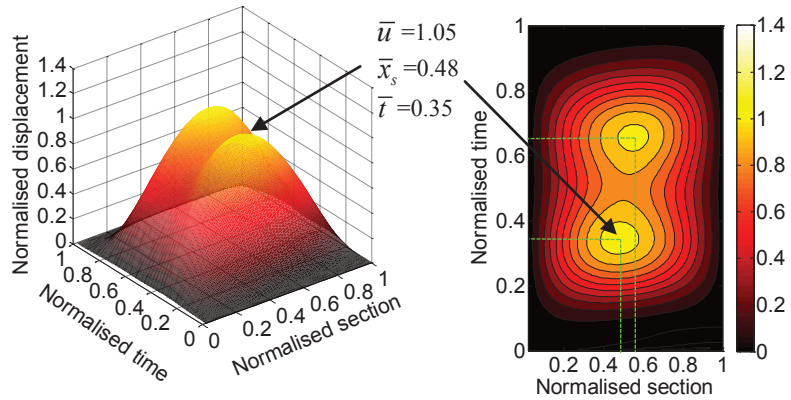

c)

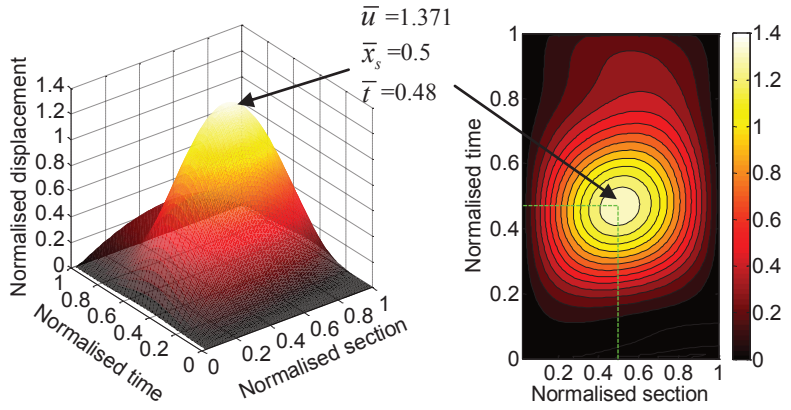

Fig. 4 : Normalized displacement versus normalized section and normalized time for a beam with $\beta = 0.02$: a) $\alpha = 0.1$, b) $\alpha = 0.2$ and c) $\alpha = 0.3$

Figure_5
Click here to download Figure: Figure 5.docx

a)

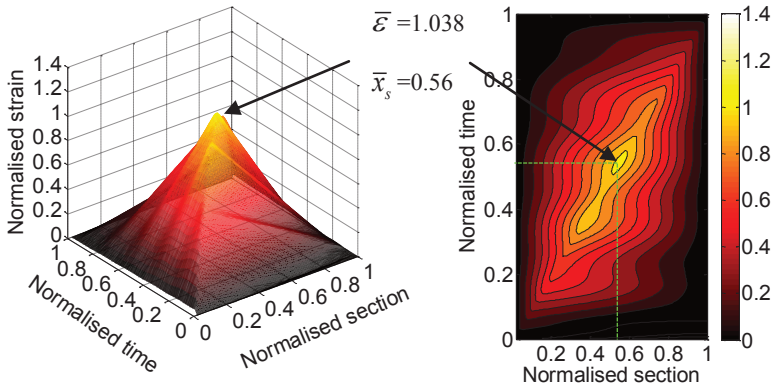

b)

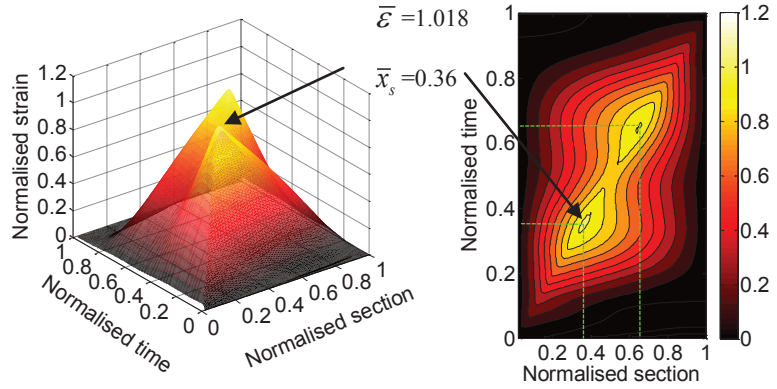

c)

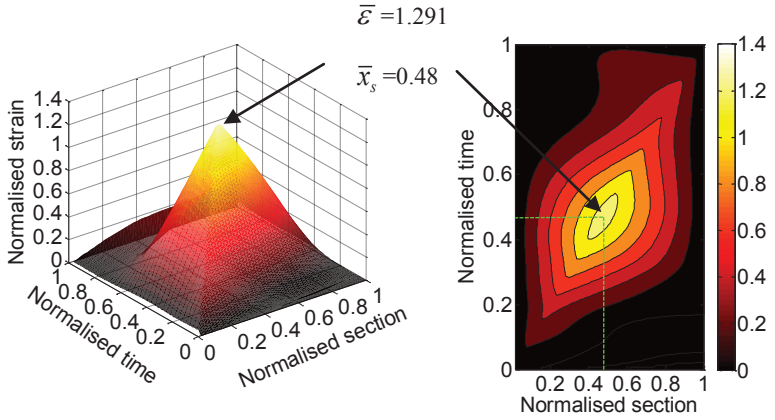

Fig. 5. Normalized strain at the bottom fibbers versus normalized section and normalized time for a beam with $\beta = 0.02$: a) $\alpha = 0.1$, b) $\alpha = 0.2$ and c) $\alpha = 0.3$

Figure_6_revised
Click here to download Figure: Figure 6.docx

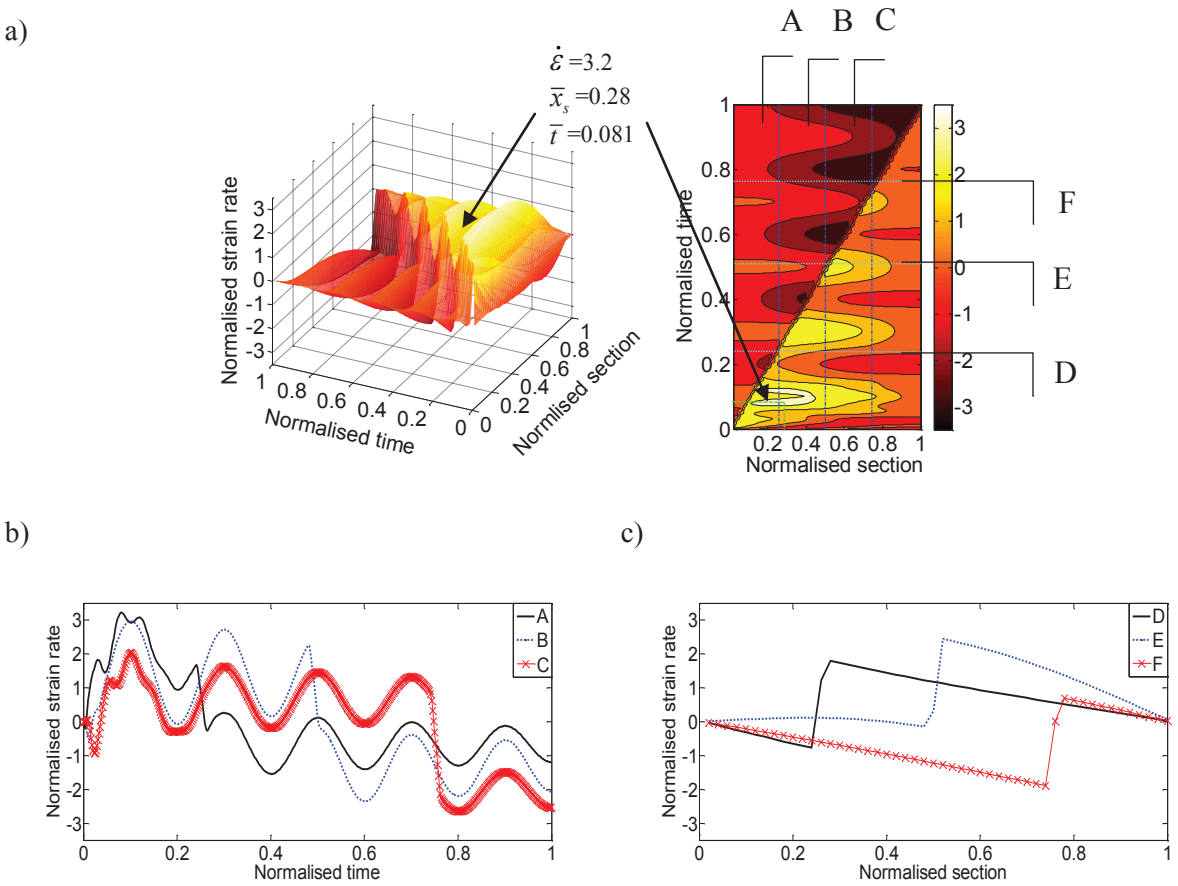

Fig. 6. a) Normalized strain rate versus normalized section and normalized time for a beam with β = 0.02 and α = 0.1, b) Vertical sections (A = 0.25 , B = 0.5 , C = 0.75), c) Horizontal sections (D = 0.25, E = 0.5, F = 0.75)

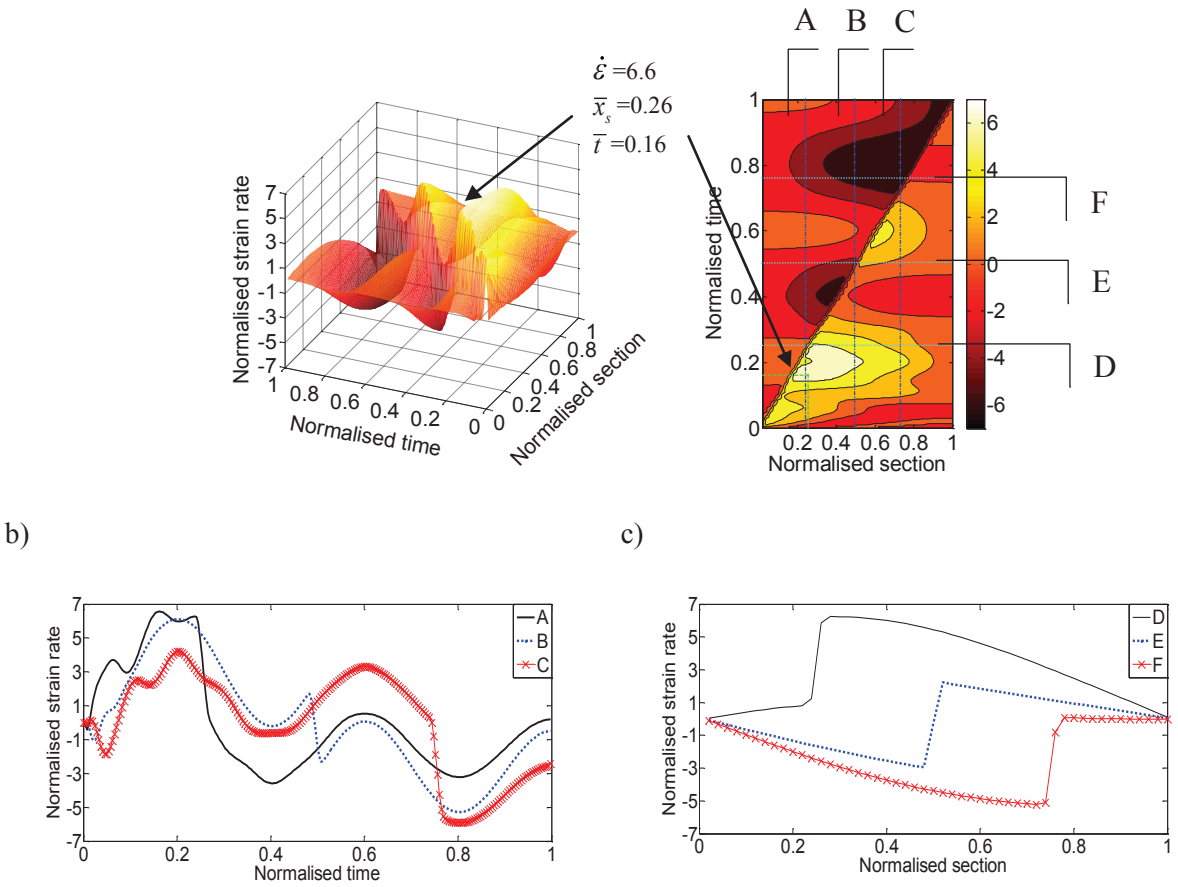

Fig. 7. a) Normalized strain rate versus normalized section and normalized time for a beam with β = 0.02 and α = 0.2, b) Vertical sections (A = 0.25 , B = 0.5 , C = 0.75), c) Horizontal sections (D = 0.25, E = 0.5, F = 0.75)

Figure_8_revised
Click here to download Figure: Figure 8.docx

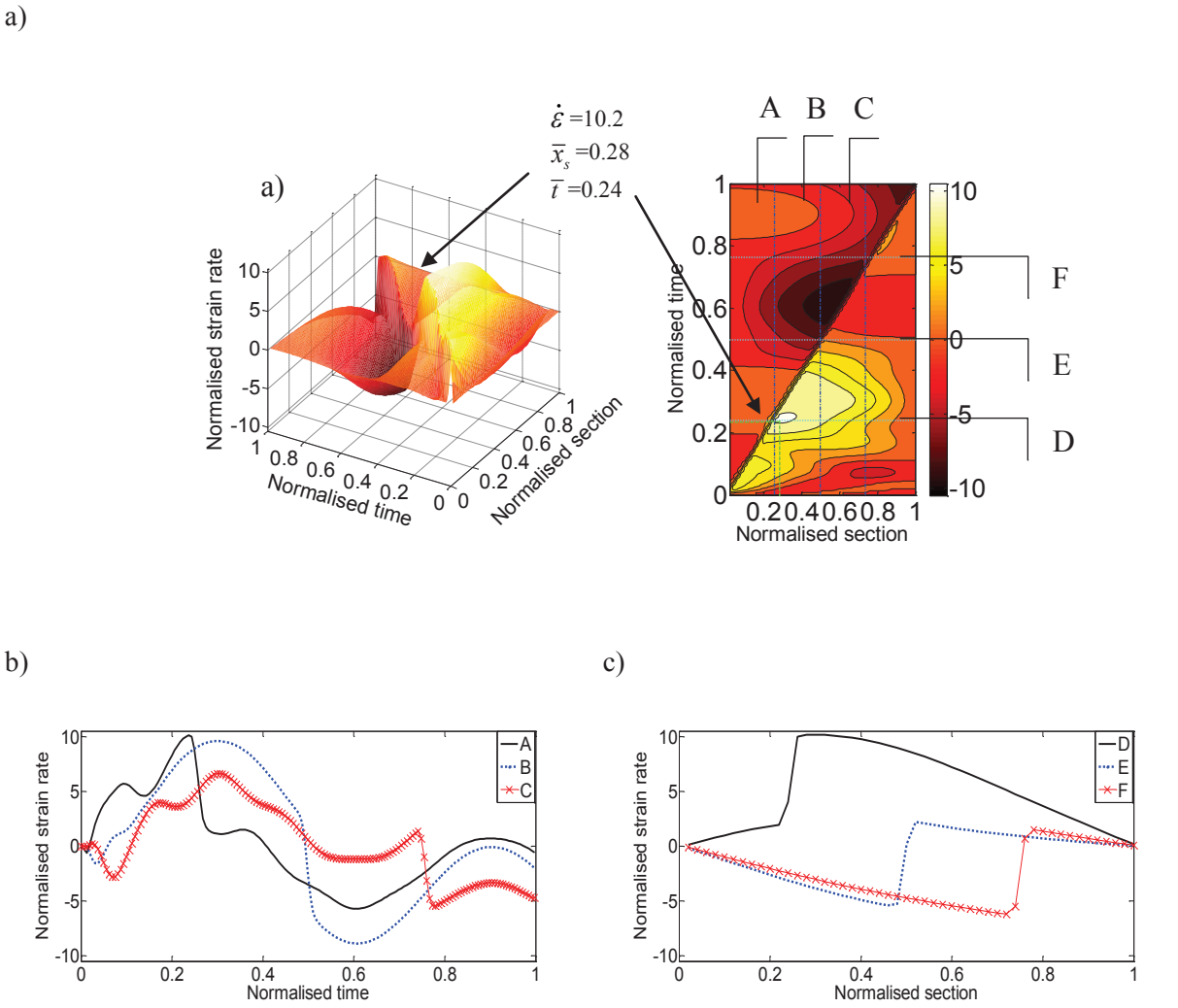

Fig. 8. a) Normalized strain rate versus normalized section and normalized time for a beam with β = 0.02 and α = 0.3, b) Vertical sections (A = 0.25 , B = 0.5 , C = 0.75), c) Horizontal sections (D = 0.25, E = 0.5, F = 0.75)

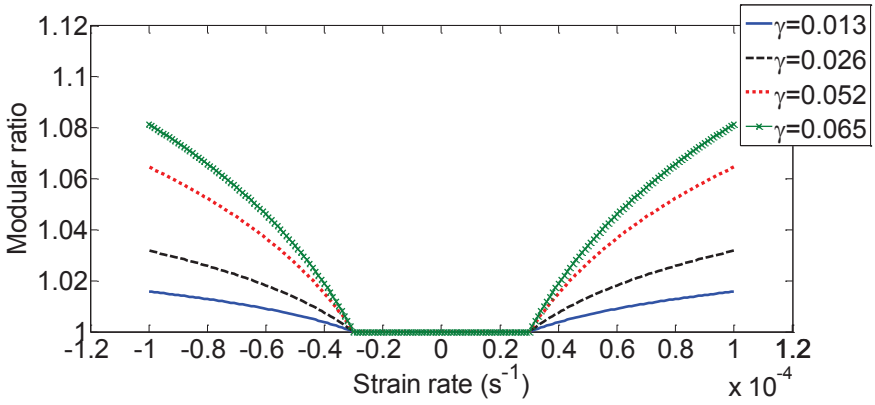

Fig. 9. Ratio of 'dynamic' to'static' modulus of elasticity versus strain rate for different γ values

Figure_10_revised
Click here to download Figure: Figure 10.docx

a)

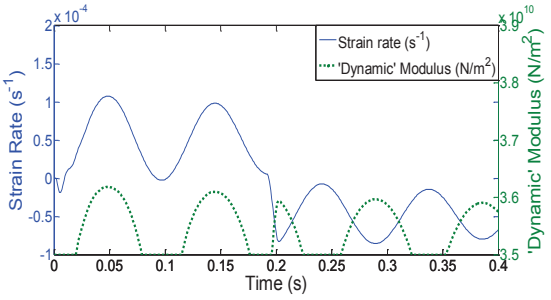

b)

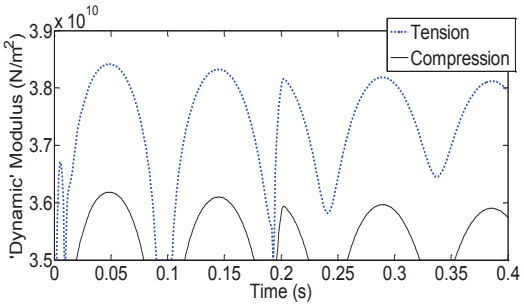

Fig. 10. Variation of moduli with time at mid-span element for $\gamma = 0.026$: (a) comparison of modulus and strain rate in compression, (b) comparison of moduli in tension and compression

Figure_11_revised
Click here to download Figure: Figure 11.docx

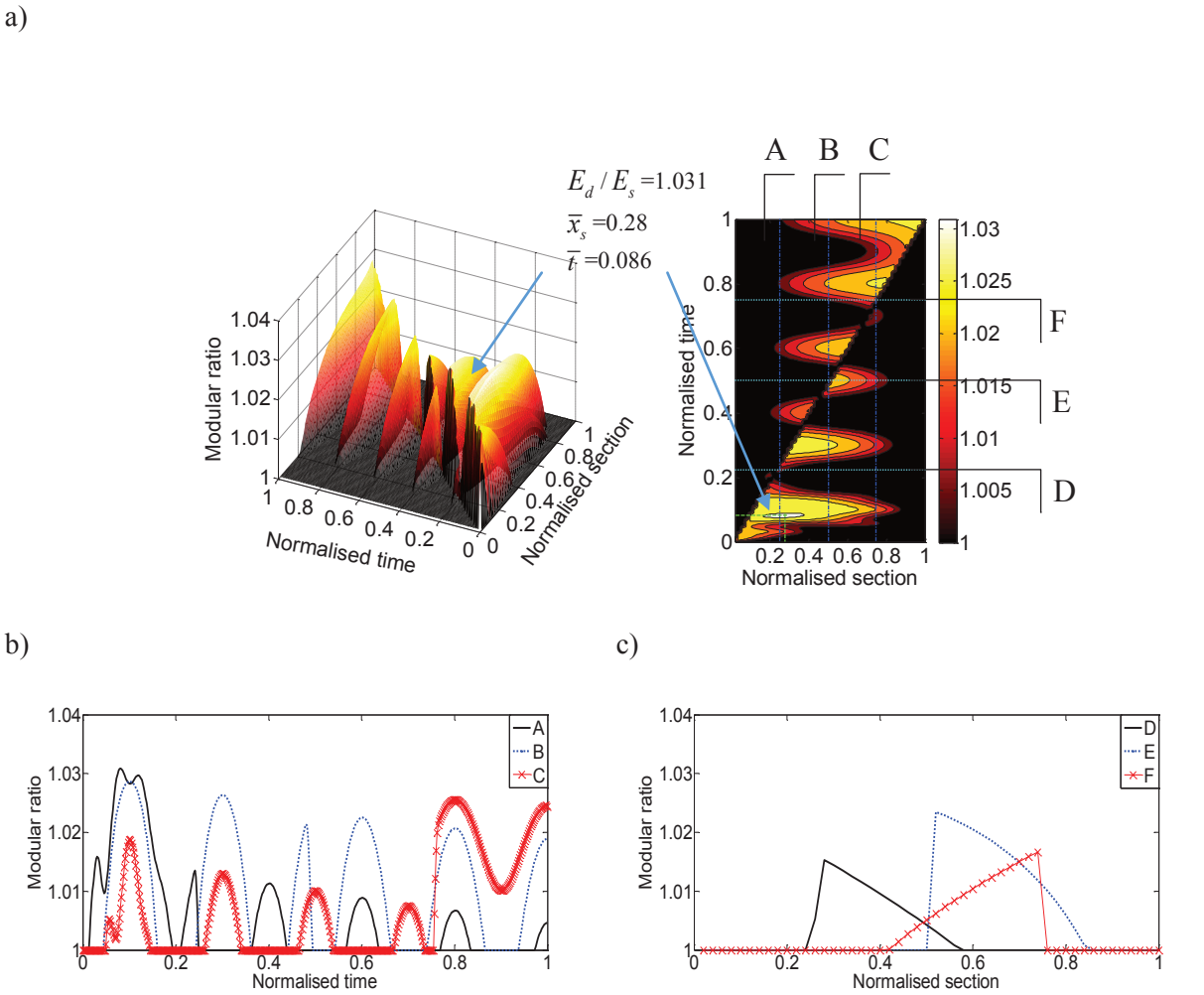

Fig. 11 a) Modular ratio versus normalized time and normalized section, β = 0.02, γ = 0.026, α = 0.1, b) Vertical sections (A = 0.25, B = 0.5 and C = 0.75), c) Horizontal sections (D = 0.25, E = 0.5 and F = 0.75)

Figure_12_revised
Click here to download Figure: Figure 12.docx

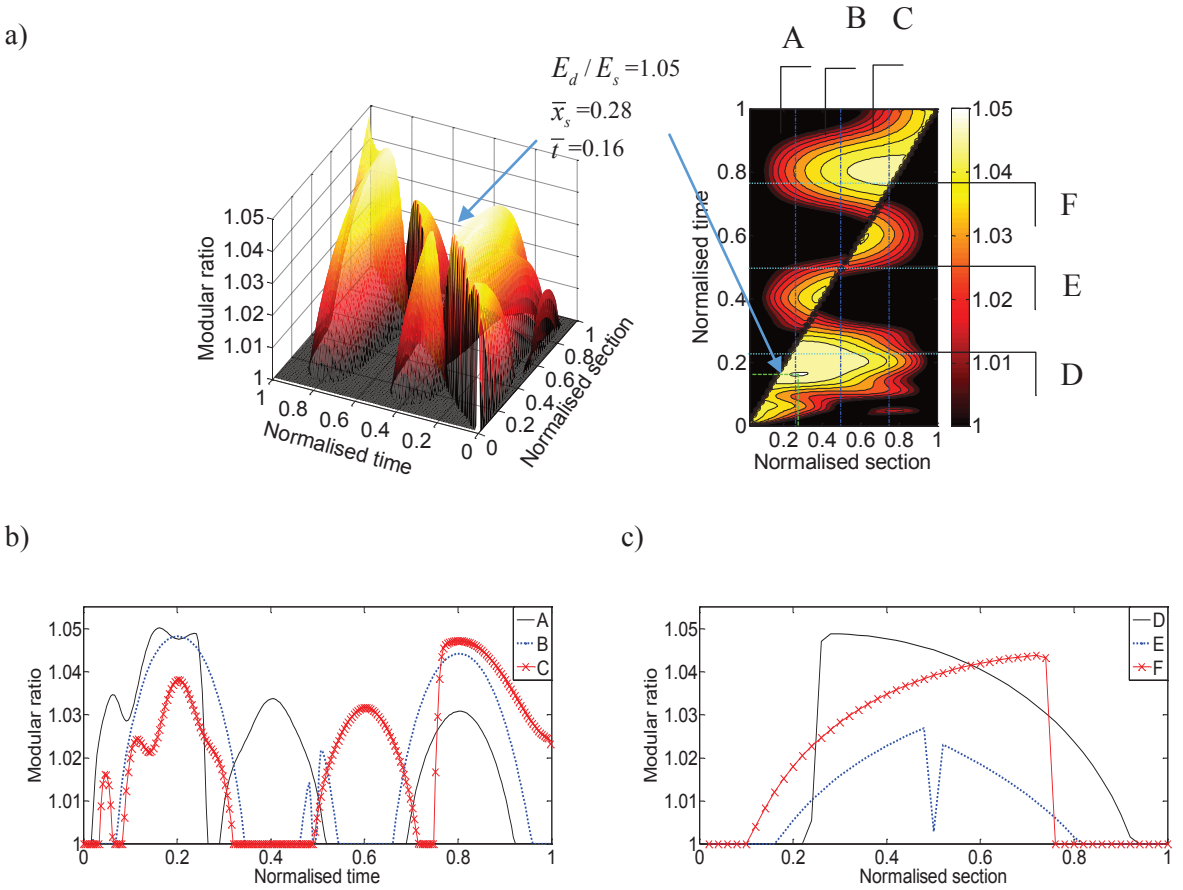

Fig. 12 a) Modular ratio versus normalized time and normalized section, β = 0.02, γ = 0.026, α = 0.2, b) Vertical sections (A = 0.25, B = 0.5 and C = 0.75), c) Horizontal sections (D = 0.25, E = 0.5 and F = 0.75)

Figure_13_revised
Click here to download Figure: Figure 13.docx

a)

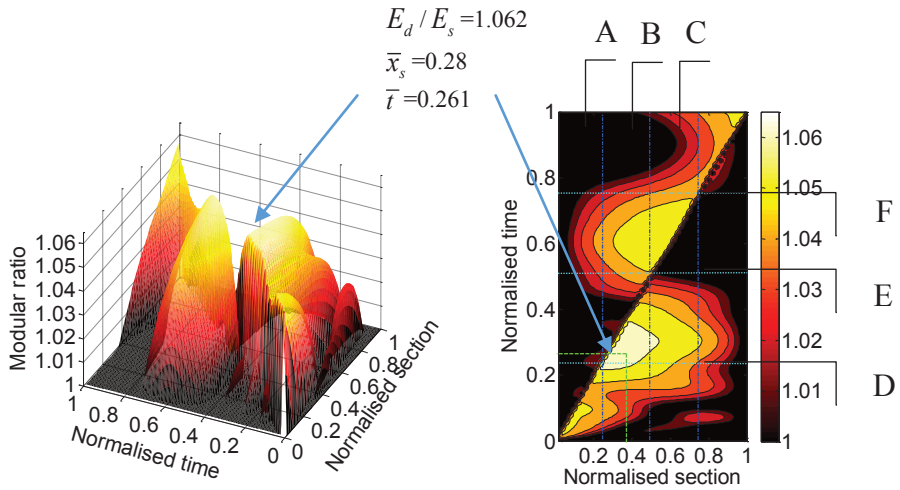

b)

c)

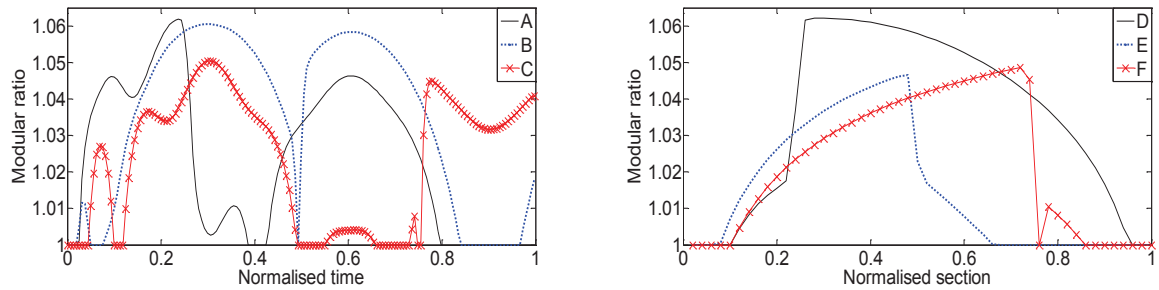

Fig. 13 a) Modular ratio versus normalized time and normalized section, β = 0.02, γ = 0.026, α = 0.3 , b)Vertical sections (A = 0.25 , B = 0.5 , C = 0.75), c) Horizontal sections (D = 0.25, E = 0.5, F = 0.75)

Figure_14
Click here to download Figure: Figure 14.docx

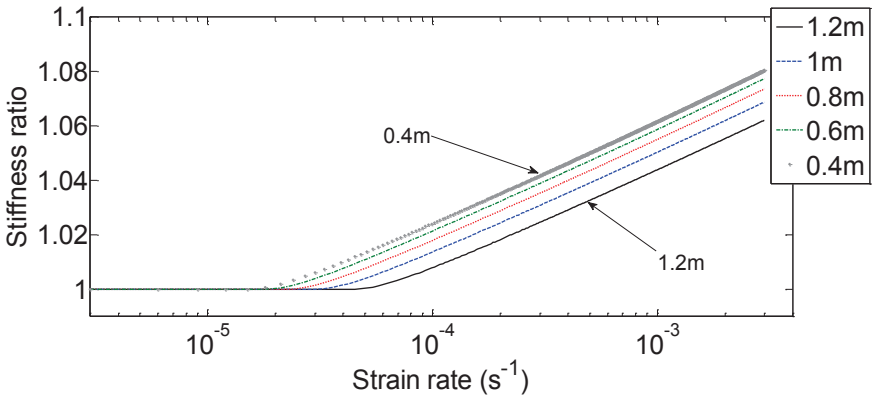

Fig. 14. Stiffness ratio versus strain rate for γ = 0.026 and different section depths.

Figure_15
Click here to download Figure: Figure 15.docx

a)

b)

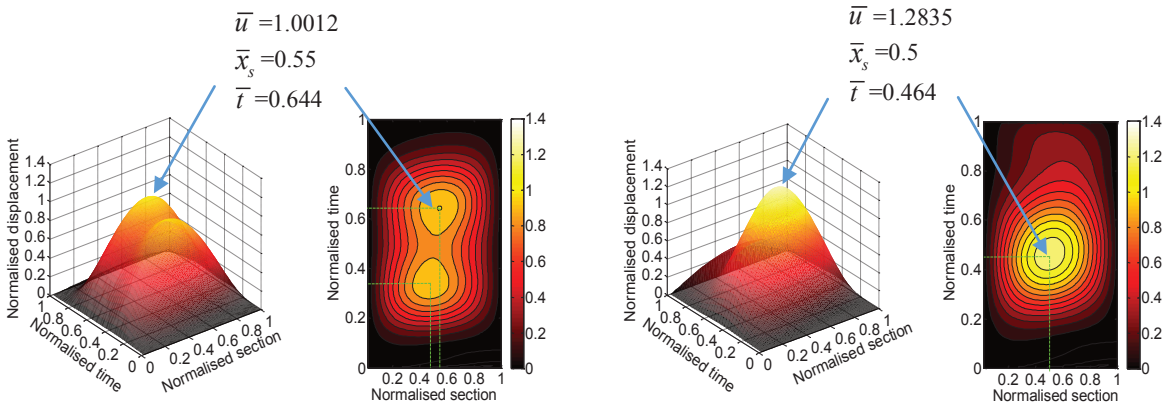

Fig. 15. Normalized displacement versus normalized time and normalized section for $\beta = 0.02$ and $\gamma = 0.026$ at speed parameter of a) $\alpha = 0.2$ and b) $\alpha = 0.3$

Figure_16
Click here to download Figure: Figure 16.docx

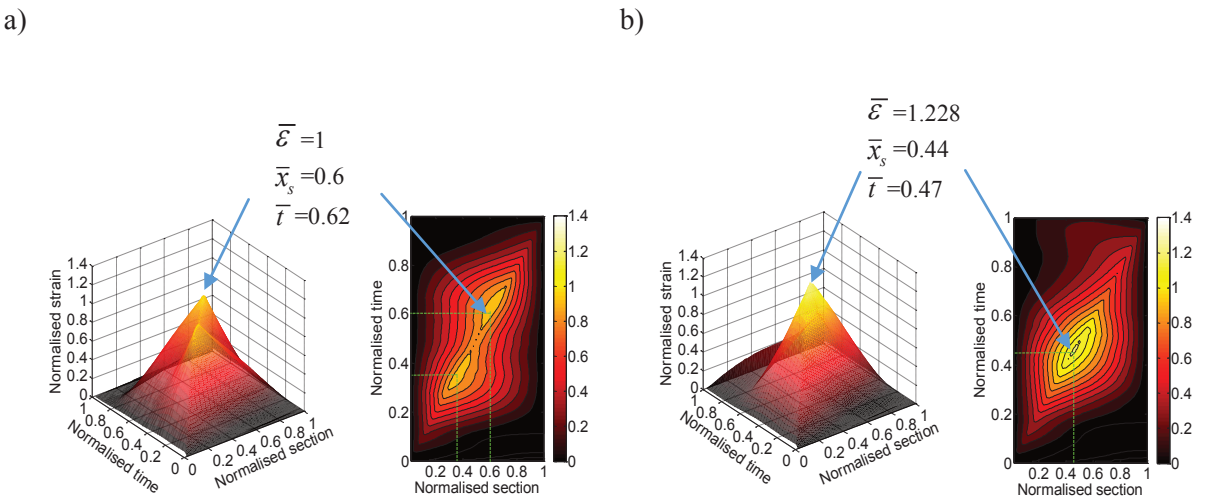

Fig. 16. Normalized strain versus normalized time and normalized section for $\beta = 0.02$ and $\gamma = 0.026$ at speed parameter of a) $\alpha = 0.2$ and b) $\alpha = 0.3$

Figure_17
Click here to download Figure: Figure 17.docx

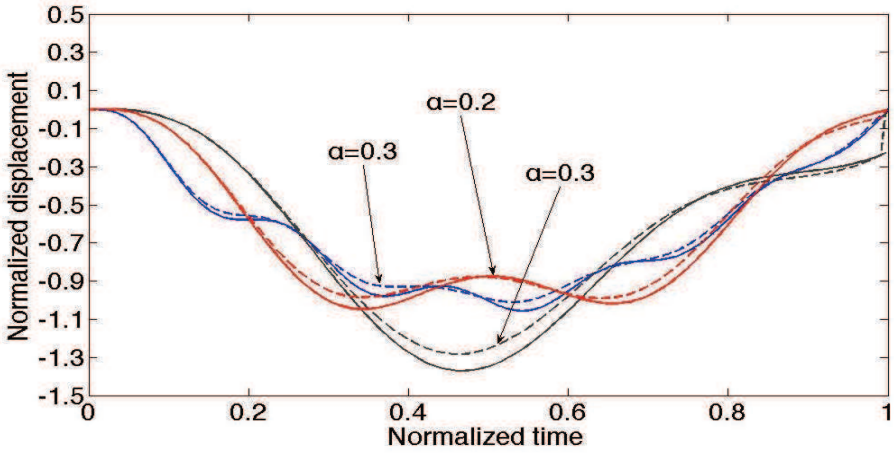

Fig. 17. Normalized displacement at mid-span section due to a 100 kN load with α = 0.1, 0.2 and 0.3, β = 0.02 and two materials: γ = 0.026 (dotted line) and (γ = 0) (solid line)

Figure_18
Click here to download Figure: Figure 18.docx

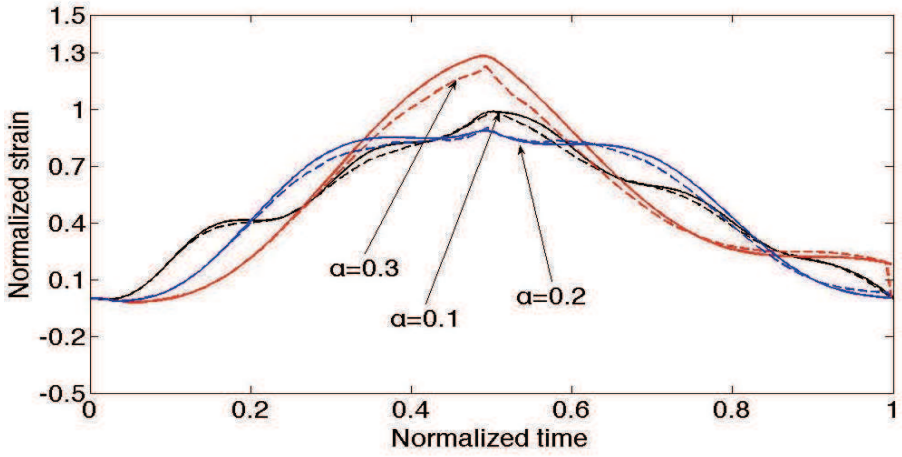

Fig. 18. Normalized strain at mid-span section due to a 100 kN load with α = 0.1, 0.2 and 0.3, β = 0.02 and two materials: γ = 0.026 (dotted line) and (γ = 0) (solid line)

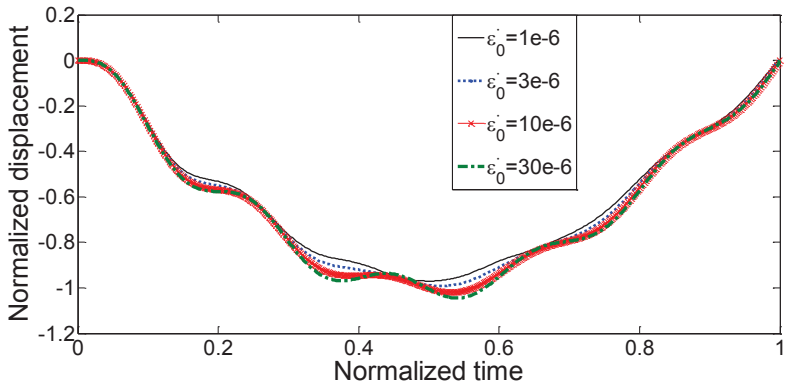

Fig. 19. Normalized displacement at mid-span using different $\dot{\varepsilon}_0$ values for $\alpha = 0.1$, $\beta = 0.02$, and $\gamma = 0.026$.

Figure_20
Click here to download Figure: Figure 20.docx

a) b)

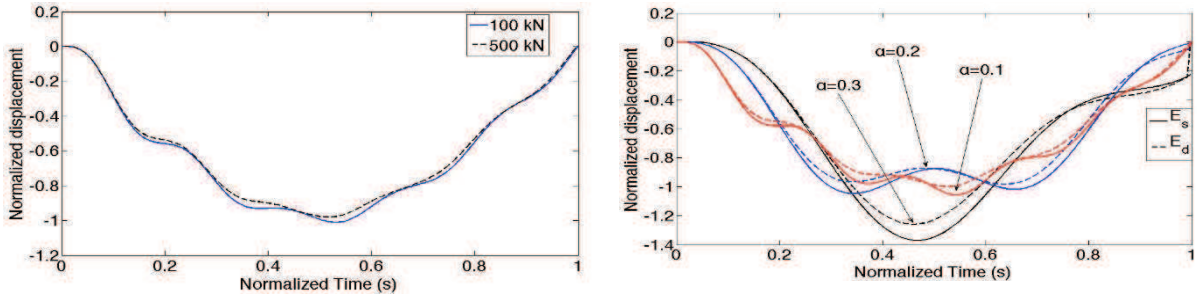

Fig. 20. Normalized displacement at mid-span with β = 0.02 traversed by loads of: (a) 100 and 500 kN at α = 0.1, with γ = 0.026 (b) 200 kN at α = 0.1, α = 0.2, and α = 0.3 and two beam materials: γ = 0 (solid line) and γ = 0.026 (dotted line)

Figure_21
Click here to download Figure: Figure 21.docx

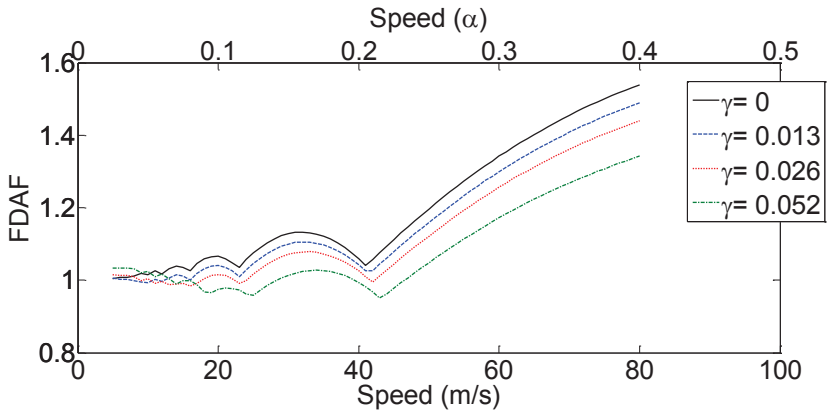

Fig. 21. FDAF of displacement at mid-span for different speed parameters and γ value

Figure_22
Click here to download Figure: Figure 22.docx

a)

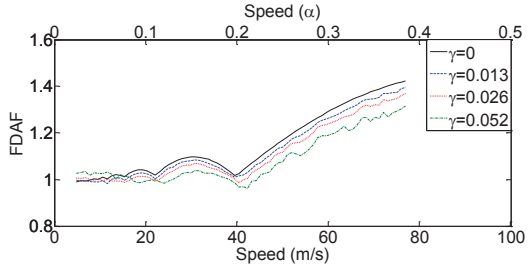

b)

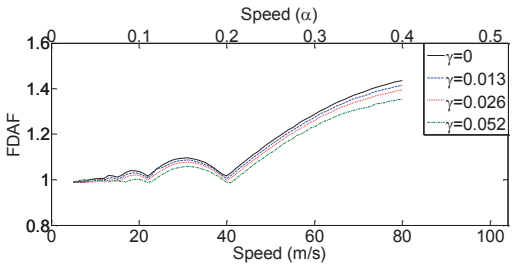

c)

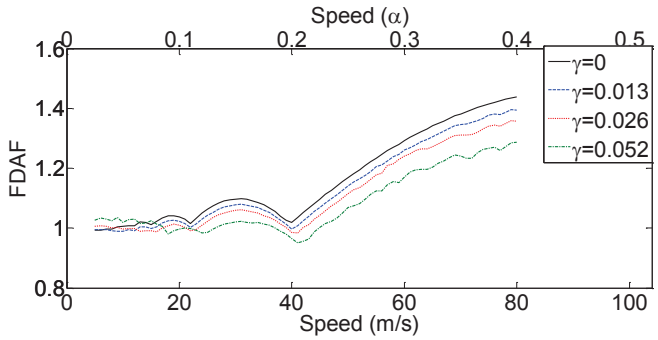

Fig. 22. FDAF of mid-span strain versus load speed; (a) 10 m span and 100 kN load, (b) 20 m span and 100 kN load, (c) 20 m span and 500 kN load; $\gamma = 0$ (solid line), $\gamma = 0.013$ (dashed line), $\gamma = 0.026$ (dotted line), $\gamma = 0.052$ (dotted line)